SURE Project: Spectroscopic Charaterisation of Silica-Gold Nanoshells

Duc Le*

(Dated: August 20, 2004)

Gold coated, silica core nanoshells of dimensions 100nm were synthesised using molecular self-assembly, and chemical reduction synthesis techniques. These were analysised using a UV-visible spectrophotometer, and the result compared with Mie theory.

I. INTRODUCTION

Metal nanoshells are a type of nanoparticle composed of a silica core, and a metallic coating. Their usual geometry is shown in Figure 1. These particles have excited interest due to their remarkable optical properties. In common with metal colloids, they show distinctive absorption peaks at specific wavelengths due to surface plasmon resonance. However, unlike bare metal colloids, the wavelengths at which resonance occurs can be 'tuned' by changing the core radius and coating thickness. One application of this is in medicine, where it is hoped that nanoshells with absorption peaks in the near-infrared can be attached to cancerous tumours. Thereafter they can be excited by lasers to heat up and kill the tumours [1]. Recent work by Halas et al. has resulted in a simple chemical synthesis technique of these particles which allows the core radius and shell thicknesses to be selected by changing the concentrations of the chemicals involved [2, 3]. Using this technique, I produced nanoshells of various dimensions, which were analysed using a UV-

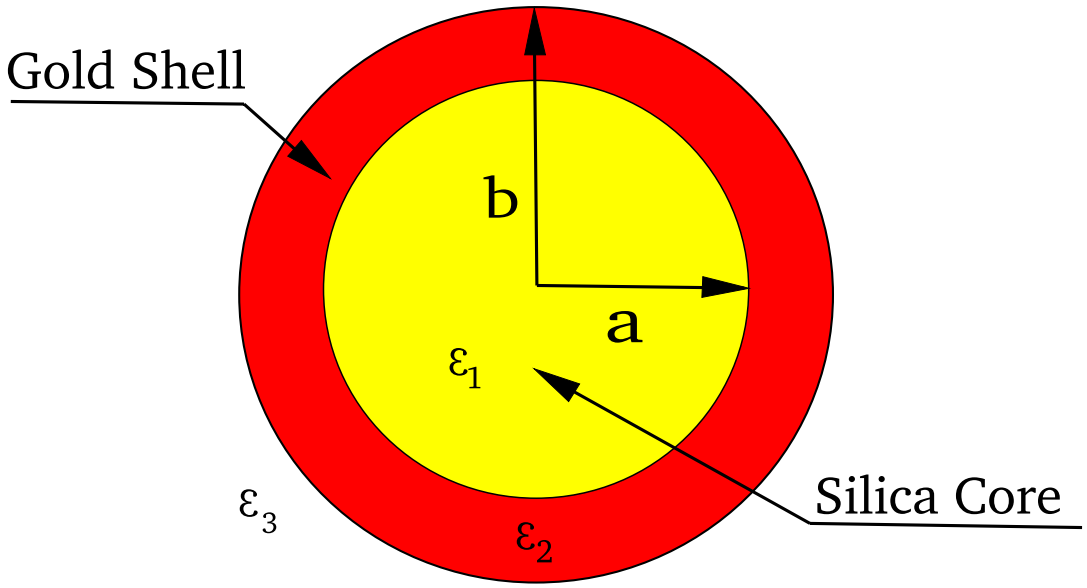

FIG. 1: *Nanoshell geometry*

*Electronic address: mdl27@cam.ac.uk

visible spectrophotometer. These results were then compared with the predictions of Mie theory, the classical theory of light scattering from small spherical particles. An atomic force micrograph was also taken of the nanoshells to determine their sizes.

II. THEORETICAL BACKGROUND

An exact solution of Maxwell's equations for spherical boundary conditions was first developed nearly a century ago, and is usually attributed to Gustav Mie, although others such as Peter Debye and Hendrik Lorentz also constructed similar solutions at the same time [4]. An outline mathematical derivation is given in Appendix VI. For our purpose in using Mie theory to compare our spectrophotometric results, we require the extinction cross-section:

$$C_{ext} = \frac{2\pi}{k^2} \sum_{n=1}^{\infty} (2n+1) \Re\{a_n + b_n\} \tag{1}$$

where k is the wave number of the scattered wave, a_n and b_n are the scattering coefficients. The extinction cross-section is a measure of the combined effects of absorption and scattering of light by the particle . It can be loosely interpreted as the "shadow" cast by the nanoshells on our detector. It is related to the absorbance by [6]:

$$A = \log_{10}\left(\frac{1}{1 - NC_{ext}}\right) \tag{2}$$

where N is the nanoshells number density in solution. Hence we can see that the absorbance is a maximum when the extinction cross-section is maximum.

As shown in Appendix VI, in Mie theory the electric and magnetic fields are expressed as infinite sums over the vector spherical harmonics, and the harmonics for the scattered fields are weighted by the coefficients a_n and b_n (equation 17). We can interpret these vector spherical harmonics as representing normal modes of the nanoshell, with the two modes for each n corresponding to *transverse magnetic* and *transverse electric* modes, in which there is no radial electric and magnetic fields respectively. For the case of a nanoshell of core radius a and total radius b, the coefficients are given by:

$$a_n = \frac{\psi_n(y)[\psi_n'(m_2 y) - A_n \chi_n'(m_2 y)] - m_2 \psi_n'(y)[\psi_n(m_2 y) - A_n \chi_n(m_2 y)]}{\xi_n(y)[\psi_n'(m_2 y) - A_n \chi_n'(m_2 y)] - m_2 \xi_n'(y)[\psi_n(m_2 y) - A_n \chi_n(m_2 y)]} \tag{3}$$

$$b_n = \frac{m_2 \psi_n(y)[\psi_n'(m_2 y) - B_n \chi_n'(m_2 y)] - \psi_n'(y)[\psi_n(m_2 y) - B_n \chi_n(m_2 y)]}{m_2 \xi_n(y)[\psi_n'(m_2 y) - B_n \chi_n'(m_2 y)] - \xi_n'(y)[\psi_n(m_2 y) - B_n \chi_n(m_2 y)]} \tag{4}$$

$$A_n = \frac{m_2 \psi_n(m_2 x)\psi_n'(m_1 x) - m_1 \psi_n'(m_2 x)\psi_n(m_1 x)}{m_2 \chi_n(m_2 x)\psi_n'(m_1 x) - m_1 \chi_n'(m_2 x)\psi_n(m_1 x)}$$

$$B_n = \frac{m_2 \psi_n(m_1 x)\psi_n'(m_2 x) - m_1 \psi_n'(m_2 x)\psi_n(m_1 x)}{m_2 \chi_n(m_2 x)\psi_n'(m_1 x) - m_1 \chi_n'(m_1 x)\psi_n(m_2 x)}$$

where $x = ka = \frac{2\pi N a}{\lambda}$ and $y = ka = \frac{2\pi N b}{\lambda}$ is the size parameter of the core and shell respectively, and m_1 and m_2 is the relative refractive index of the core and shell to that of the medium. $\psi_n(z)$, χ_n and ξ_n are the Ricatti-Bessel functions, and the primes indicate differentiation with respect to the argument. A single mode a_n or b_n will therefore dominate over all the others if the denominator in that coefficient is zero. Now if we take the limit of small particles, and expand the Ricatti-Bessel

functions in power series, we see that the denominator of b_n will never vanish for any n, but that of a_n will vanish as $x \to 0$, $y \to 0$ if:

$$m_2^2 = -\frac{n+1}{n} \quad (n = 1, 2, \ldots) \tag{5}$$

For the a_1 electric dipole mode, then we require $m_2^2 = -2$. Since the refractive index is generally complex, we have $m = i\sqrt{2}$. In terms of the complex dielectric function ($\varepsilon = N^2$), this condition is $\varepsilon_2 = -2\varepsilon_m$ where ε_m is the dielectric function of the medium. Since the dielectric function is a function of frequency, the frequency at which this condition is met is called the *Fröhlich frequency* ω_F, and the a_1 often called the Fröhlich mode after Herbert Fröhlich who first obtained an expression for this frequency for dielectric crystals [7]. The effect of finite size and the gold coating over the silica core is to change the condition 5, and hence shift the Fröhlich frequency. It can be shown that for the nanoshell we require:

$$\varepsilon_1 = -2\varepsilon_2 \left(\frac{\varepsilon_2(1-f) + (2+f)}{\varepsilon_2(2f+1) + 2(1-f)} \right) \tag{6}$$

where $f = a^3/b^3$ is the volume fraction of the core to the total volume. Thus the shift in frequency depends on the dielectric constant of both core and shell and the ratio of their sizes.

In must be noted here that whilst we have used the language of classical electrodynamics to describe the optical properties of nanoshells, that both the classical and quantum mechanical descriptions are *quantitatively* the same. Indeed, the electrodynamical treatment includes the necessary quantum mechanics within it in the form of the dielectric function, which for many materials cannot be adequately described by classical models.

However, the use of quantum mechanical terms in the literature is extensive. In particular, what we have refered to as normal modes are termed *surface plasmons* and interpreted to mean the quantised excitations of charge density imparted by the material absorbing an incident photon. In bulk materials, a plasmon would have energy $\hbar\omega_p$ where $\omega_p = Ne^2/m\varepsilon_0$ is the plasma frequency of the material. However, in small particles, the energy of the plasmon becomes $\hbar\omega_F$, which can be shown for simple free electron metals to be some fraction of the bulk plasmon energy, hence the term surface plasmon.

III. EXPERIMENTAL METHODS

Spherical silica nanoparticles were synthesised first using Stöber's method [8], in which ammonia is used as a catalyst for the hydrolysis of tetraethylorthosilicate ($Si(OC_2H_5)_4$), or TEOS, in a solution of absolute ethanol. The reaction of water with TEOS produces a singly hydrolysed TEOS monomer, $(OH)Si(OC_2H_5)_3$, which subsequently condenses to form silica. The overall reaction is:

$$Si(OC_3H_5)_4 + 2H_2O \rightarrow SiO_2 + C_3H_5OH$$

It is thought that the condensation causes the continuous nucleation of insoluble silica particles which later aggregate to form the final spherical nanoparticles [9]. Thus the final size of these particles depends to both the nucleation and aggregation rates. Large particles will be produced at low nucleation and high aggregation rates, which corresponds to a low water concentration, denoted $[H_2O]$, but high TEOS concentration $[TEOS]$, and vice versa. Thus a major factor in the size of the silica spheres is the ratio $R = [H_2O]/[TEOS]$ [10]. In addition, the alcohol solution

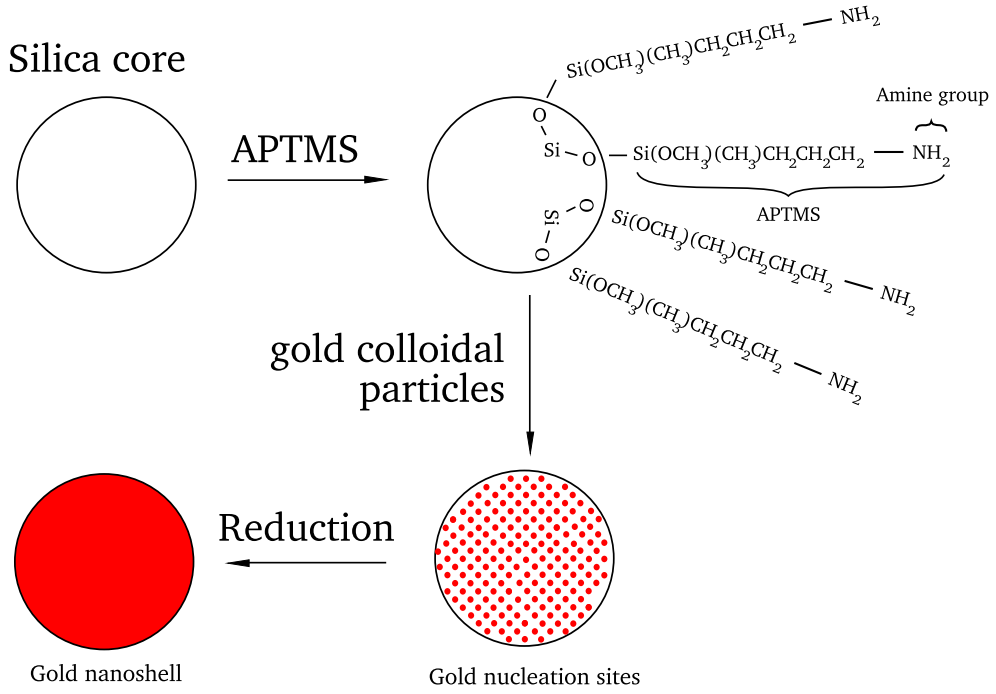

FIG. 2: *Steps involved in the synthesis of silica-gold nanoshells*

in which the hydrolysis takes place also affects the size, with ethanol producing particles about twice as large as methanol due to a lower supersaturation ratio of the single hydrolysed monomer which causes a lower nucleation rate [11]. For our purpose, to synthesise spherical silica cores of $\approx 100nm$ radius, $3m$ of 30% ammonia solution in water, and $1.5ml$ of TEOS was added to $50ml$ of ethanol, and stired vigourously. The chemicals were obtained from Sigma Aldrich, and used as received.

The silica core thus produced was then coated with 3-aminopropyltrimethoxysilane, APTMS. About $30\mu l$ of APTMS was added to the $50ml$ of silica particle solution just made. The APTMS is adsorbed onto the silica surface, forming a siloxane bond between a silicon atom at one end of the APTMS molecule and an oxygen atom on the silica particle. As a result the other end of the APTMS molecule with an amine (HNH_2) group always points away from the silica core, as shown in Figure 2. These amine group acts as attachment point for colloidal gold particles, due to their affinity for gold [12]. A separate solution of gold colloids, about $2nm$ in radius, was prepared by the reduction of chloroauric acid, $HClAu_4$ with tetrakis(hydroxymethyl)phosphonium chloride, or THPC, in a sodium hydroxide $NaOH(aq)$ solution. $2ml$ of $1\%HAuCl_4$ was added to a solution of $45ml$ high grade water, $0.5ml$ $1MNaOH$ and $1ml$ THCP. $5ml$ of this colloidal solution was added to $0.5ml$ of APTMS-functionalised silica core solution, resulting in silica nanoparticles with perhaps 25% of their surface covered by colloidal gold.

These nanoparticles formed a suspension, which was allowed to settle. Thereafter, the excess ethanol was pipetted out, and the particles redispersed in high grade water. Subsequently a reducible gold solution, made by adding $1.5ml$ of $1\%HAuCl_4$ to $25mg$ of potassium carbonate in $100ml$ of high grade water, was added to the gold-attached silica solution. $10\mu l$ of formaldehyde was then added to suddenly increase the pH, bring the gold out of solution, to self assemble on to gold already on the silica core, completing the gold coating [3]. Different thickness of gold shells were obtained by varying the concentration of the $HAuCl_4$ solution added.

The nanoshell solutions were analysed as made using a Perkin-Elmer Model 330 spectrophotometer. For the atomic force microscope analysis, the nanoshell solution was pipetted onto a tilted silicon substrate and left to evaporate to form a thin film.

IV. RESULTS

The spectra for representative nanoshell solutions made is shown in Figure 3, along with a theoretical fit. The fit was calculated using equations 1, 2, 3 and 4. For the required complex refractive index of gold, the experimental data of Johnson and Christy was used [13], and for silica that of Malitson [14]. These data were further modified to take into account the dimensions of the nanoshell, which is of the same order or smaller than the electron mean free path in gold($\approx 11nm$), where collisions with the shell boundaries may become more important. Using the simple Drude theory [4], the dielectric constant is modified by:

$$\varepsilon = \varepsilon_{exp} + \frac{\omega_p^2}{\omega^2 + i\omega\gamma_{bulk}} - \frac{\omega_p^2}{\omega^2 + i\omega(\gamma_{bulk} + v_F/(b-a))} \tag{7}$$

where ε_{exp} is the experimentally obtained dielectric constant, γ_{bulk} is the bulk collisional frequency, v_F is the Fermi velocity.

In addition, the theoretical fit presumes a gaussian size distribution for the nanoshells, which is calculated by weighting the extinction cross-sections at different sizes accordingly, and then summing these contributions.

Finally, Figure 4 shows an atomic force micrograph of a nanoshell sample, with a histogram size distribution in Figure 5

Whilst Figure 5 suggests that the nanoshells are quite small, the Mie theory fits in Figure 3 shows that the particles should be at least twice as large as was infered from the AFM data. The histogram in Figure 5 was calculated by the SCION Image program, which requires a strong contrast between particles. Because of the clustering of the nanoshells in a 'ridge' near the left hand side of Figure 4, the contrast may not have been high enough. In addition the program requires a 'threshold' height in order to determine the boundary of the particles. Since the particles on the ridge is much higher than that elsewhere, it is probable that the program discounted many particles that did not pass the threshold. In light of these factors, it is difficult to estimate the errors in Figure 5, but it's probably fair to say that it may not be representative of the overall size distribution of the nanoshells.

V. FURTHER WORK

The nanoshells that I have produced have had relatively large size distribution, and thick shells. As seen in Figure 3, this results in a broad absorbance peak, which is not shifted very far from the Fröhlich frequency of pure gold($\approx 520nm$). For the medical purposes given in Section I, we

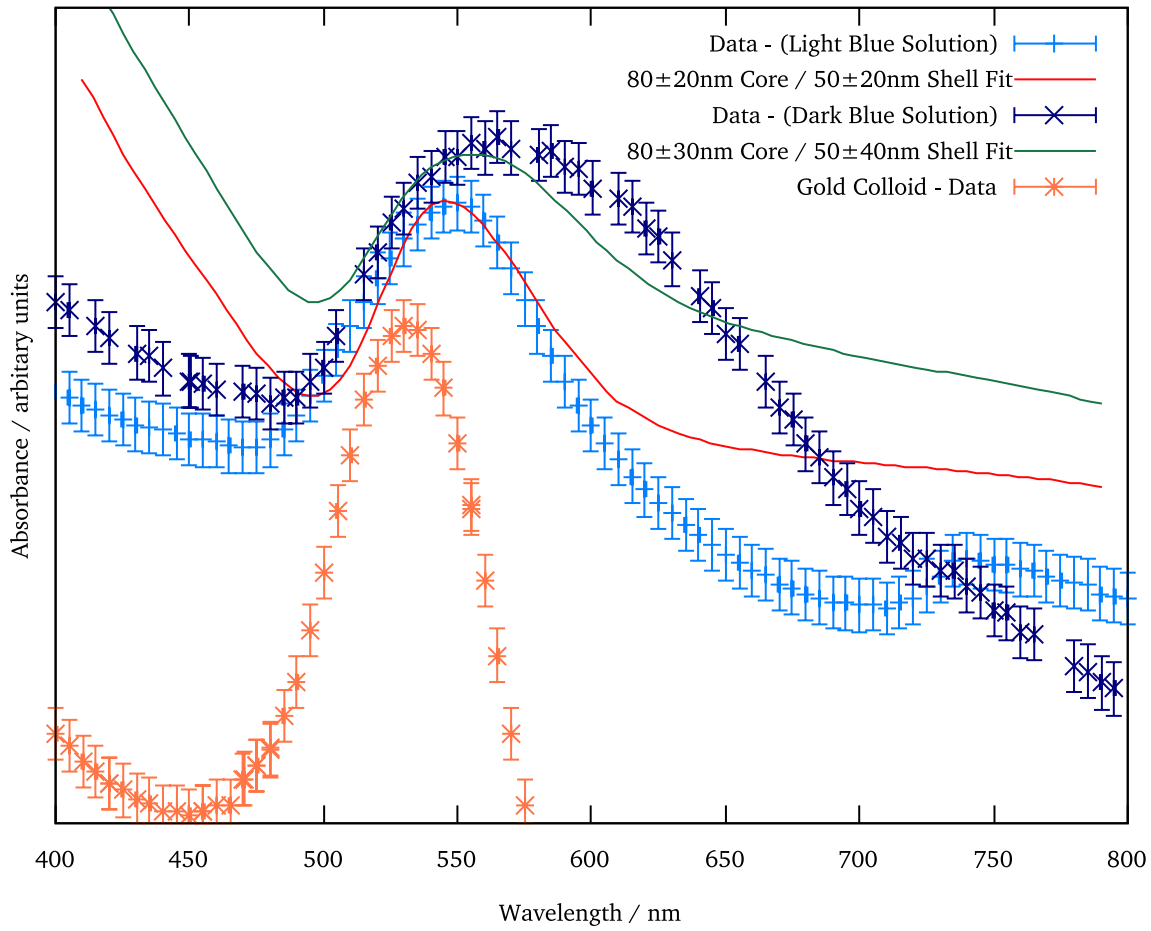

FIG. 3: *Nanoshell absorption spectrum and calculated Mie theory fits.*

would need a much larger shift, corresponding to a thinner shell, and larger core radius. Therefore the next step is to try to synthesise such nanoshells. In addition to gold, silica-core, silver shelled particles have been made elsewhere [15], as are gold-core, silver-shelled particles [16], so an investigation of similar combinations may be of interest.

---

[1] J.L. West et al., Proc. Nat. Acad. Sci. USA **100** 13549-13554 (2003)

[2] S.J. Oldenburg, R.D. Averitt, S.L. Westcott, N.J. Halas, Chem. Phys. Lett. **288** 243-247 (1998)

[3] T. Pham, J.B. Jackson, N.J. Halas, T.R. Lee, Langmuir **18** 4915-4920 (2002)

[4] C.F. Bohren, D.R. Huffman *Absorption and Scattering of Light by Small Particles*, John Wiley & Sons (1983)

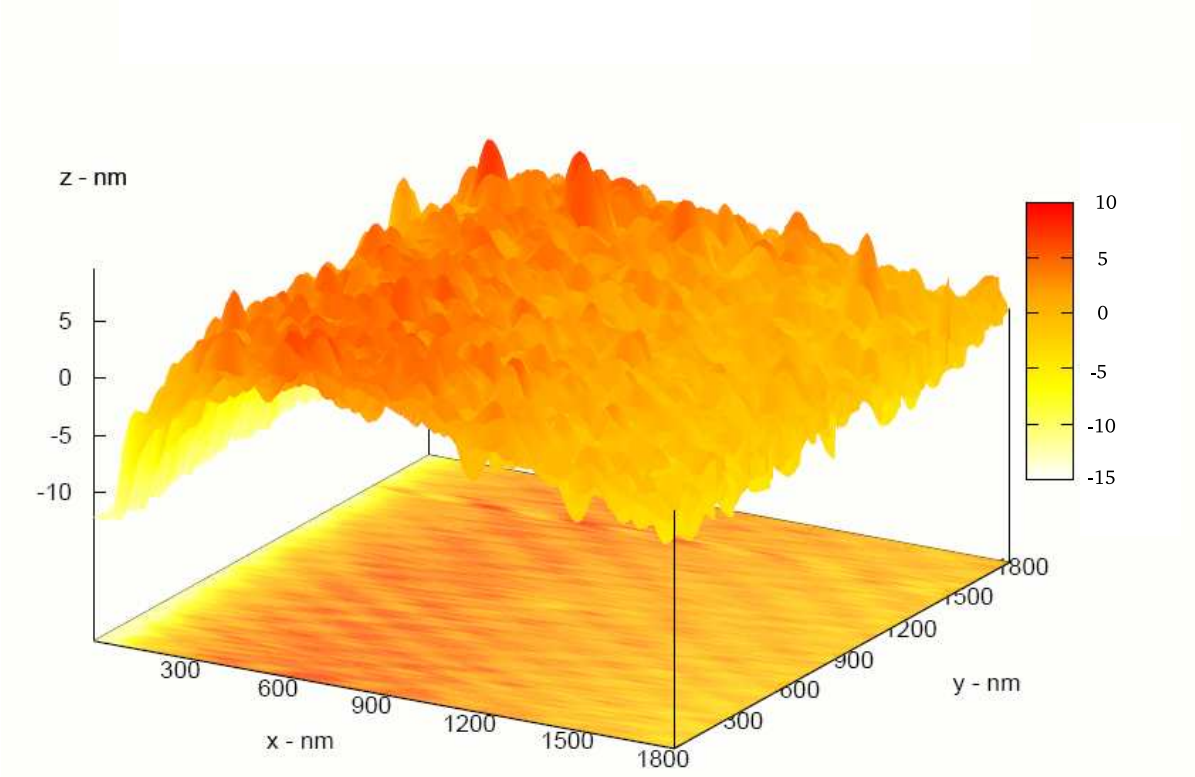

FIG. 4: *Atomic force micrograph of a silica-core, gold-shell nanoshell. The shells tend to form clusters like that on the left side of the graph.*

[5] J.A. Stratton, *Electromagnetic Theory*, McGraw-Hill (1941)
[6] S.W. Kennerly, J.W. Little, R.J. Warmack, T.L. Ferrell, Phys. Rev. B **29** 2926-2929 (1984)
[7] H. Fröhlich *Theory of Dielectrics*, Oxford University Press (1949)
[8] W. Stöber, A. Fink, E. Bohn, J. Colloid Interface Sci. **26** 62-69 (1968)
[9] K. Lee, J-L Look, M.T. Harris, A.V. McCormick, J. Colloid Interface Sci., **194** 78-88 (1997)
[10] S.K. Park, K.D. Kim, H.T. Kim, Colloids and Surfaces A **197** 7-17 (2002)
[11] D. L. Green et al., J. Colloid Interface Sci. **266** 346-358 (2003)
[12] T. Sato, D. Brown, B.F.G. Johnson, Chem. Commun. **11** 1007 - 1008 (1997)
[13] P.B. Johnson, R.W. Christy, Phys. Rev. B **6** 4370-4378 (1972)
[14] L.H. Malitson, J. Opt. Soc. Am. **55** 1205-1209 (1965)
[15] J.B. Jackson, N.J. Halas, J. Phys. Chem. B **105** 2743-2746 (2001)
[16] Y. Kim, R.C. Johnson, J. Li, J.T. Hupp, G.C. Schatz, Chem. Phys. Lett, **352** 421-428 (2002)

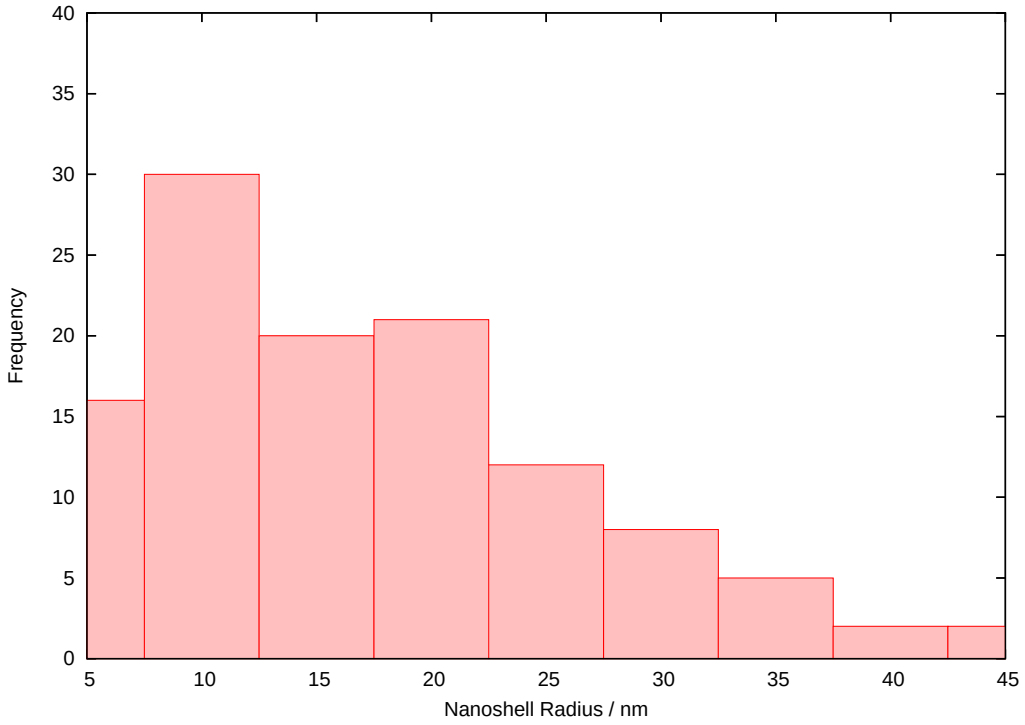

FIG. 5: *Histogram of particle size from atomic force micrograph. The size distribution was determined using the SCION Image software. The low values for the radius is due to the lack of resolution in the micrograph, and probably the contrast between the clustered nanoshells and unclustered caused many to be miscounted.*

Appendix

VI. MIE THEORY DERIVATION

In the treatment that follows, we will be using the approach of Stratton [5]. We first take the incident fields as time-harmonic, with an $exp(-i\omega t)$ dependence, so that the Maxwell's third and four equations means that the electric and magnetic fields are not independent, and both satisfy the vector wave equation:

$$\begin{aligned} \nabla \times \mathbf{E} &= i\omega\mu\mathbf{H} \\ \nabla \times \mathbf{H} &= -i\omega\varepsilon\mathbf{E} \\ \nabla^2\mathbf{E} + k^2\mathbf{E} &= 0 \\ \nabla^2\mathbf{H} + k^2\mathbf{H} &= 0 \end{aligned} \tag{8}$$

Now, we can express the electric and magnetic fields as infinite sums over the *vector spherical harmonics*, denoted by **M** and **N**, and constructed from a scalar *generating function* ψ as follows:

$$\mathbf{M} = \nabla \times (\mathbf{c}\psi)$$
$$\mathbf{N} = \frac{\nabla \times \mathbf{M}}{k} \tag{9}$$

where **c** is an arbitary constant vector called the *pilot* vector, an $k^2 = \omega^2 \varepsilon \mu$ is the wave-number of the electromagnetic wave. These vector harmonics have properties similar to the electric and magnetic fields: They are divergence free, and the curl of one is proportional to the other (in the case of time-harmonic fields). In addition, they satisfy the vector wave equation if the generating funtion also satisfies the scalar wave equation:

$$\nabla^2 \psi + k^2 \psi = 0 \tag{10}$$

The solutions of this equation in spherical polars is well known, and is:

$$\psi_{emn} = \cos(m\phi) P_n^m(\cos\theta) z_n(kr)$$
$$\psi_{omn} = \sin(m\phi) P_n^m(\cos\theta) z_n(kr) \tag{11}$$

The subscripts *e* and *o* denote *even* and *odd*, P_n^m is the associated Legendre function of the first kind of degree n and order m, and z_n is any of the four spherical Bessel functions j_n, y_n, $h_n^{(1)}$, $h_n^{(2)}$ (first, second and third kind respectively). These functions form a complete set, so the vector harmonics **M** and **N** generated from ψ_{emn} and ψ_{omn} will also form a complete set, and will be solution to the vector wave equation. Hence any solutions to the vector wave equations (i.e. the electric and magnetic fields) can be expressed as an infinite series in the vector harmonics:

$$\mathbf{E} = \sum_{m=0}^{\infty} \sum_{n=0}^{\infty} B_{emn}\mathbf{M}_{emn} + B_{omn}\mathbf{M}_{omn} + A_{emn}\mathbf{N}_{emn} + A_{omn}\mathbf{N}_{omn} \tag{12}$$

Another property of the vector harmonics is that they are orthogonal:

$$\langle \mathbf{M}_{em'n'} | \mathbf{M}_{omn} \rangle = \langle \mathbf{N}_{em'n'} | \mathbf{N}_{omn} \rangle = \langle \mathbf{M}_{om'n'} | \mathbf{N}_{omn} \rangle = \langle \mathbf{M}_{em'n'} | \mathbf{N}_{emn} \rangle = 0 \ \text{(all } m, n, m', n')$$

$$\langle \mathbf{M}_{emn} | \mathbf{M}_{emn'} \rangle = \langle \mathbf{M}_{omn} | \mathbf{M}_{omn'} \rangle = 0 \quad (\text{for } n \neq n' \text{ and } m \neq 0)$$
$$\langle \mathbf{N}_{emn} | \mathbf{N}_{emn'} \rangle = \langle \mathbf{N}_{omn} | \mathbf{N}_{omn'} \rangle = 0 \quad (\text{for } n \neq n' \text{ and } m \neq 0) \tag{13}$$

where the brackets indicate an inner product $\int_0^{2\pi} \int_0^{\pi} \sin\theta d\theta d\phi$. We can thus determine the coefficients A and B in equations 12 by using the inner products to pick out individual terms with different values of m, and n in turn.

Using equations 9 and 11 we can obtain expressions for the spherical harmonics in component form (in spherical polars). If we further assume that the light incident on the nanoshell is plane polarised, then equating the components and picking out terms in the inner products we can get the desired expansion:

$$\mathbf{E}_i = E_0 \sum_{n=1}^{\infty} i^n \frac{2n+1}{n(n+1)} (\mathbf{M}_{o1n}^{(1)} - i\mathbf{N}_{e1n}^{(1)})$$

$$\mathbf{H}_i = \frac{-k}{\omega\mu} E_0 \sum_{n=1}^{\infty} i^n \frac{2n+1}{n(n+1)} (\mathbf{M}_{e1n}^{(1)} + i\mathbf{N}_{o1n}^{(1)}) \tag{14}$$

The superscript $^{(1)}$ indicates that a Bessel function of the first kind (j_n) was used in the generating function to ensure that the fields remain finite at the origin, in the centre of the nanoshell, since $y_n \to -\infty$ as $r \to 0$.

Now that we have an expression for the incident (plane wave) fields in terms of the vector harmonics, we can use the boundary conditions for EM waves in a media ($\mathbf{E}_{||}$ and $\mathbf{H}_{||}$ - the component of the field parallel to the boundaries - must be continuous across the boundary) to express the field inside the shell ($\mathbf{E}_2$, $\mathbf{H}_2$) and core of the particle ($\mathbf{E}_1$, $\mathbf{H}_1$), and the field scattered by the particle ($\mathbf{E}_s$, $\mathbf{H}_s$):

$$\mathbf{E}_1 = E_o \sum_{n=1}^{\infty} i^n \frac{2n+1}{n(n+1)} (c_n \mathbf{M}_{o1n}^{(1)} - i d_n \mathbf{N}_{e1n}^{(1)})$$

$$\mathbf{H}_1 = \frac{-k}{\omega\mu} E_o \sum_{n=1}^{\infty} i^n \frac{2n+1}{n(n+1)} (d_n \mathbf{M}_{e1n}^{(1)} - i c_n \mathbf{N}_{o1n}^{(1)}) \tag{15}$$

$$\mathbf{E}_2 = E_o \sum_{n=1}^{\infty} i^n \frac{2n+1}{n(n+1)} (f_n \mathbf{M}_{o1n}^{(1)} - i g_n \mathbf{N}_{e1n}^{(1)} + v_n \mathbf{M}_{o1n}^{(2)} - i w_n \mathbf{N}_{e1n}^{(2)})$$

$$\mathbf{H}_2 = \frac{-k}{\omega\mu} E_o \sum_{n=1}^{\infty} i^n \frac{2n+1}{n(n+1)} (g_n \mathbf{M}_{e1n}^{(1)} + i f_n \mathbf{N}_{o1n}^{(1)} + w_n \mathbf{M}_{e1n}^{(2)} + i v_n \mathbf{N}_{o1n}^{(2)}) \tag{16}$$

where c_n, d_n, g_n, f_n, v_n, w_n are coefficients to be determined. In the shell both bessel functions of the first and second order are finite, so we have to include both (denoted by the superscripts) in the series expansions.

Finally we have the scattered fields:

$$\mathbf{E}_s = E_o \sum_{n=1}^{\infty} i^n \frac{2n+1}{n(n+1)} (-b_n \mathbf{M}_{o1n}^{(3)} + i a_n \mathbf{N}_{e1n}^{(3)})$$

$$\mathbf{H}_s = \frac{k}{\omega\mu} E_o \sum_{n=1}^{\infty} i^n \frac{2n+1}{n(n+1)} (-a_n \mathbf{M}_{e1n}^{(1)} + i b_n \mathbf{N}_{o1n}^{(1)}) \tag{17}$$

where a_n and b_n are the scattering coefficients to be determined. The superscript $^{(3)}$ indicates that the vector harmonics are derived from the Hankel function of the first kind, $h_n^{(1)}(kr) = j_n(kr) + iy_n(kr)$ whose asymptotic behaviour corresponds to an *outgoing* wave, unlike the Hankel function of the second kind, which corresponds to an incoming wave.

To determine the coefficients above, we need to substitute these series expansions into expressions for the boundary conditions in component form. This yields a system of eight equations in the eight coefficients which can then be solved to yield, the scattering coefficients:

$$a_n = \frac{\psi_n(y)[\psi_n'(m_2 y) - A_n \chi_n'(m_2 y)] - m_2 \psi_n'(y)[\psi_n(m_2 y) - A_n \chi_n(m_2 y)]}{\xi_n(y)[\psi_n'(m_2 y) - A_n \chi_n'(m_2 y)] - m_2 \xi_n'(y)[\psi_n(m_2 y) - A_n \chi_n(m_2 y)]}$$

$$b_n = \frac{m_2 \psi_n(y)[\psi_n'(m_2 y) - B_n \chi_n'(m_2 y)] - \psi_n'(y)[\psi_n(m_2 y) - B_n \chi_n(m_2 y)]}{m_2 \xi_n(y)[\psi_n'(m_2 y) - B_n \chi_n'(m_2 y)] - \xi_n'(y)[\psi_n(m_2 y) - B_n \chi_n(m_2 y)]}$$

$$A_n = \frac{m_2 \psi_n(m_2 x)\psi_n'(m_1 x) - m_1 \psi_n'(m_2 x)\psi_n(m_1 x)}{m_2 \chi_n(m_2 x)\psi_n'(m_1 x) - m_1 \chi_n'(m_2 x)\psi_n(m_1 x)}$$

$$B_n = \frac{m_2\psi_n(m_1x)\psi_n'(m_2x) - m_1\psi_n'(m_2x)\psi_n(m_1x)}{m_2\chi_n(m_2x)\psi_n'(m_1x) - m_1\chi_n'(m_1x)\psi_n(m_2x)} \tag{18}$$

where $x = ka = \frac{2\pi Na}{\lambda}$ and $y = ka = \frac{2\pi Nb}{\lambda}$ is the size parameter of the core (radius a) and shell (total radius b) respectively, and m_1 and m_2 is the relative refractive index of the core and shell to that of the medium.

A. Cross Section

Now that we have explicit expressions for the scattered fields, we can work out the scattered intensities and cross-sections. The power scattered is given by integrating the Poynting vector ($\mathbf{S} = \mathbf{E} \times \mathbf{H}$) over the surface of an imaginery sphere that much larger than the particle:

$$W_s = \int_A \mathbf{S}_s \cdot \mathbf{r} dA$$

where $\mathbf{S}_s = \mathbf{E}_s \times \mathbf{H}_s$ is the scattered Poynting vector, $\mathbf{r}$ is the radial unit vector in spherical polars. In components:

$$W_s = \frac{1}{2}\Re \int_0^{2\pi} \int_0^{\pi} (E_{s\phi}H_{s\theta}^* - E_{s\theta}H_{s\phi}^*) r^2 \sin\theta d\theta d\phi$$

where r is the radius of the imaginery sphere. We now substitute in the expressions for the scattered fields in component forms (as series expansions in terms of the normal modes) and intergrate term by term:

$$W_s = \frac{\pi |E_o|^2}{k\omega\mu} \sum_{n=1}^{\infty} (2n+1)(|a_n|^2 + |b_n|^2)$$

and the cross sections is:

$$C_s = \frac{W_s}{I_i} = \frac{2\pi}{k^2} \sum_{n=1}^{\infty} (2n+1)(|a_n|^2 + |b_n|^2)$$

since $I_i = |E_o|^2$, and $k^2 = \omega^2 \varepsilon \mu$.

In addition to the light that is scattered by the particle, some of the incident light is also absorbed. The sum of the absorption and scattering is the *extinction*, with the extinction power given by: $W_{ext} = W_a + W_s$. The absorbed power is:

$$W_a = \int_A (\mathbf{E}_1 \times \mathbf{H}_1) \cdot \mathbf{r} dA$$

substituting in the expressions for $\mathbf{E}_1$ and $\mathbf{H}_1$ in terms of the scattered and incident fields from the four boundary conditions equations above, we get the expression for the extinction power in component form:

$$W_{ext} = \frac{1}{2}\Re \int_0^{2\pi} \int_0^{\pi} (E_{i\phi}H_{s\theta}^* - E_{i\theta}H_{s\phi}^* - E_{s\theta}H_{i\phi}^* + E_{s\phi}H_{i\theta}^*) r^2 \sin\theta d\theta d\phi$$

and from this, substituting in the expressions for the field components, and integrating term by term, finally dividing by the incident amplitude, we get the extinction cross-section:

$$C_{ext} = \frac{W_{ext}}{I_i} = \frac{2\pi}{k^2} \sum_{n=1}^{\infty} (2n+1)\Re\{a_n + b_n\}$$

To a good approximation, our detector has a small enough area, and is far enough from the scattering particle, that the solid angle it subtends at the particle is negligible. Thus the scattered intensity, being proportional to the solid angle subtended at the particle is also negligible. This means that the power at the detector is

$$W \approx W_i - W_{ext} = I_i(A_{detector} - C_{ext})$$

Hence to determine C_{ext} we simply measure the incident intensity I_i without the particle, and then measure the intensity with it.